The Abdus Salam
International Centre for Theoretical Physics

United Nations
Educational, Scientific
and Cultural Organization

International Atomic
Energy Agency

World Year of PHYSICS 2005

SMR.1670 - 35

INTRODUCTION TO MICROFLUIDICS

8 - 26 August 2005

Slip or No-slip?

V. Steinberg
Weizmann Institute of Science, Israel

Strada Costiera 11, 34014 Trieste, Italy - Tel. +39 040 2240 111; Fax +39 040 224 163 - sci_info@ictp.it, www.ictp.it

Slip or no-slip?

Lecture 8

V. Steinberg

Summer School in Microfluidics,
August 8-26, 2005, ICTP, Trieste, Italy

WEIZMANN
INSTITUTE
OF SCIENCE

Introduction

In contrast with the usual picture where the velocity of a liquid or gas flow on a solid wall is zero, recent experiments have shown that simple liquids and gases may significantly slip on solid surfaces and, consequently, the no-slip condition should be replaced by a more general relation

Second-order slip laws in microchannels for helium and nitrogen

Jean Maurer, Patrick Tabeling, Pierre Joseph, and Herve Willaime
Laboratoire de Physique Statistique, Ecole Normale Supérieure, 24 rue Lhomond, 75231 Paris, France
and Microfluidics, MEMS, Nanostructures, ESPCI, 10 rue Vauquelin, 75231 Paris, France

Range of existence of slip flow regime?

Gas flow experiment in shallow micro-channel, $1.14 \pm 0.02 \mu m$ deep and 200 micron wide etched in glass and covered by silicon waver
Flow rate and pressure drop measurements are performed for He and Ni for **Kn**=0.8 and 0.6. Upper limit for slip flow is **Kn**=0.3

$$Kn \equiv \frac{\lambda}{L}$$

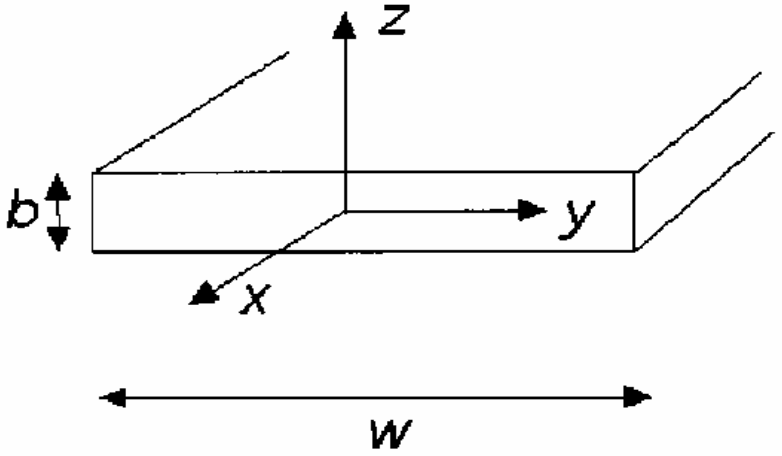

FIG. 1. Channel geometry, with the system of coordinates. Throughout the paper, we assume the channel is shallow, i.e., its depth b is much smaller than its width w, so that, except close to the sides, the fluid essentially sees two infinite parallel planes, separated by b.

The possibility that ordinary gases slip against solid walls has been proposed long ago by Maxwell. By statistical arguments, Maxwell obtained the following expression for the boundary conditions :

$$u = \frac{2-\sigma}{\sigma}\lambda\frac{\partial u}{\partial z}$$

in which ***u*** is the velocity at the walls, ***z*** the coordinate normal to the wall, and ***λ*** is the mean free path for the gas, and the accomodation factor, a fraction σ of the gas molecules that reflect diffusively against the walls (the rest undergoing specular reflection).

This condition means that gas layers slip against the wall

By working with extremely well defined channel geometries, of sizes comparable to the mean free path, the authors now have the possibility to confront, with an unprecedented degree of accuracy, such a condition with the experiment.

- **range of existence of the slip regime**
- **form of the boundary conditions**

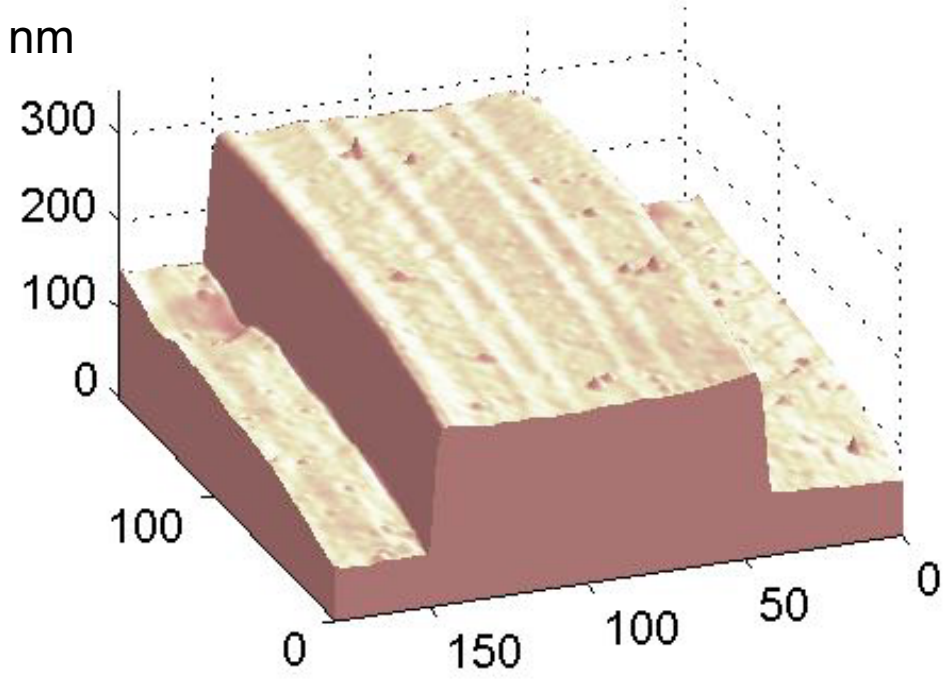

Image of channel obtained by microscopic interferometry

Fluid mechanical background: first and second order boundary conditions and Stokes approximation

$$u = \pm A_1 \lambda \frac{\partial u}{\partial z}; A_1 = \frac{2-\sigma}{\sigma}$$

$$\mathrm{Re} = Q_m / w\mu << 1 (\approx 10^{-3})$$

$$-\frac{\partial p}{\partial x} + \mu\left(\frac{\partial^2 u}{\partial x^2} + \frac{\partial^2 u}{\partial z^2}\right) = 0$$

Pressure-driven gas in slip flow regime

$$Q_m = \rho q(x) = \rho \frac{Gb^3 w}{12\mu}\left(1 + 6A_1 Kn(x)\right)$$

$$G = -dp/dx; Kn(x) = \lambda(x)/b$$

$$\lambda(x) = \frac{k_B T}{2^{1/2}\pi p(x) a^2}$$

$$p = \rho RT$$

$$P_m = 1/2(P_I + P_O), P_I = p(0); P_O = p(L)$$

$$Kn(x) = Kn\frac{P_m}{p(x)}$$

$$\left(1 + 6A_1 Kn(x)\right)\frac{\partial(p^2)}{\partial x} = -\frac{24\mu Q_m RT}{wb^3}$$

continuation

$$Q_m = \frac{\Delta P P_m w b^3}{12 \mu R T L}\left(1 + 6 A_1 Kn\right)$$

$$S \equiv \frac{12 Q_v \mu P_O L}{\Delta P P_m w b^3}$$

$$S = 1 + 6 A_1 Kn$$ **-it is a direct way to check the boundary condition**

Second-order boundary condition (transition regime)

$$u = \pm A_1 \lambda \frac{\partial u}{\partial z} - A_2 \lambda^2 \frac{\partial^2 u}{\partial z^2}$$ (Stokes eq. is solved instead of Burnett eq.)

$$S = 1 + 6 A_1 Kn + 12 A_2 Kn^2 \frac{P_m Ln(\Pi)}{\Delta P}$$

$$\Pi = \frac{P_I}{P_O}$$ (developing in powers of $\Delta P / 2P_m$)

$$S \approx 1 + 6 A_1 Kn + 12 A_2 Kn^2$$

Averaged *Kn* is the control parameter

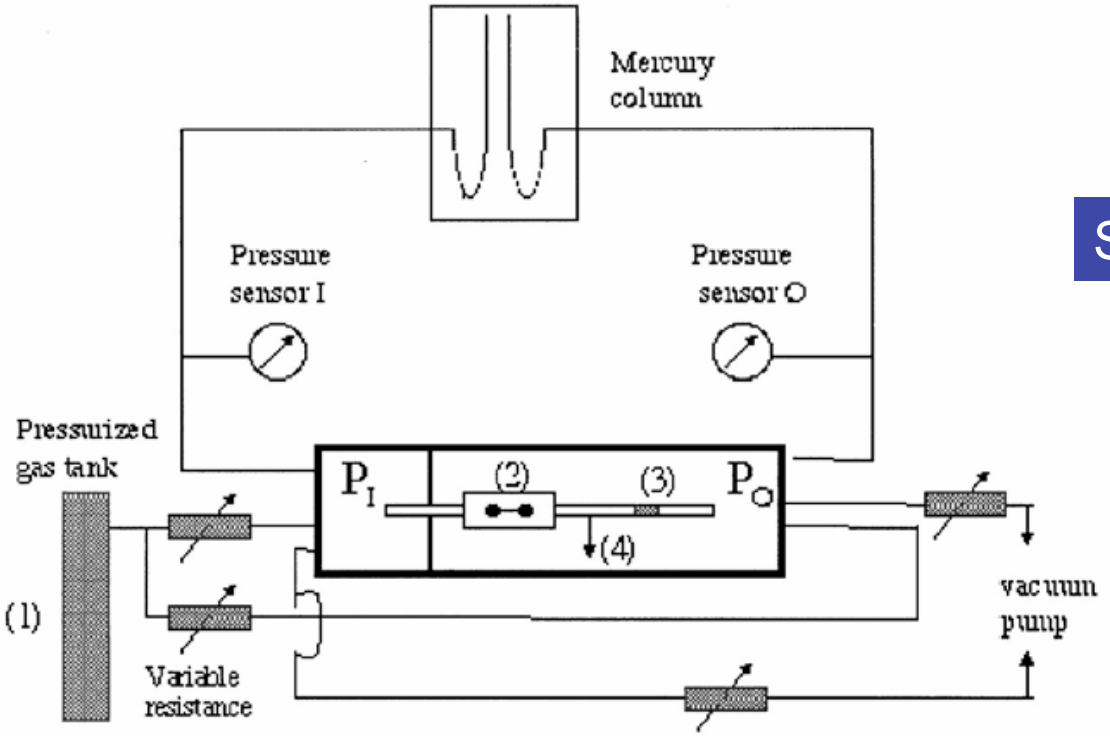

Sketch of experimental setup

Channel depth, ***b***

$$1.14 \pm 0.02\,\mu m$$

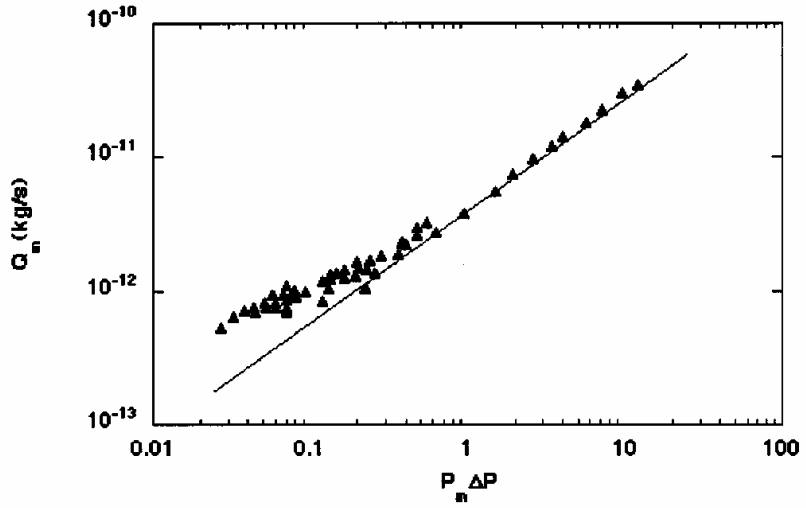

FIG. 4. Plot of the mass flow-rate as a function of the composite pressure drop $P_m \Delta P$, for helium. The full line is drawn to "guide the eyes;" it represents the evolution we expect at low Knudsen numbers.

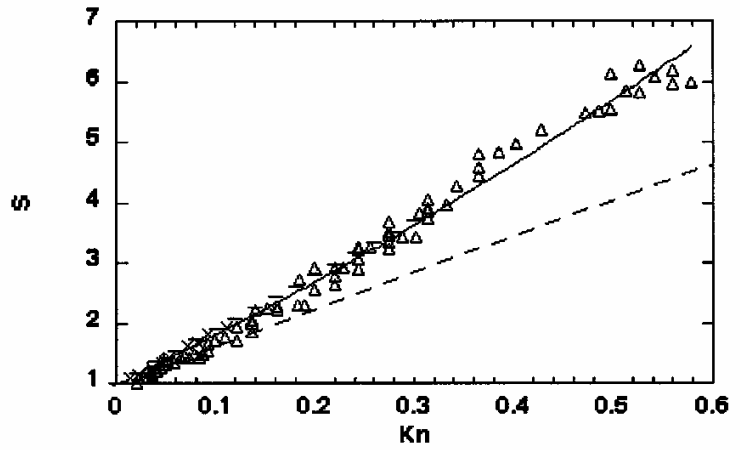

FIG. 6. Evolution of the slip coefficient S, for nitrogen. Crosses represent Colin *et al.* data, and horizontal segments are extracted from Arkilic *et al.*; the dashed line represents the full accommodation limit ($\sigma=1$), without second-order effects. The full line is the fit by a polynom of degree 2.

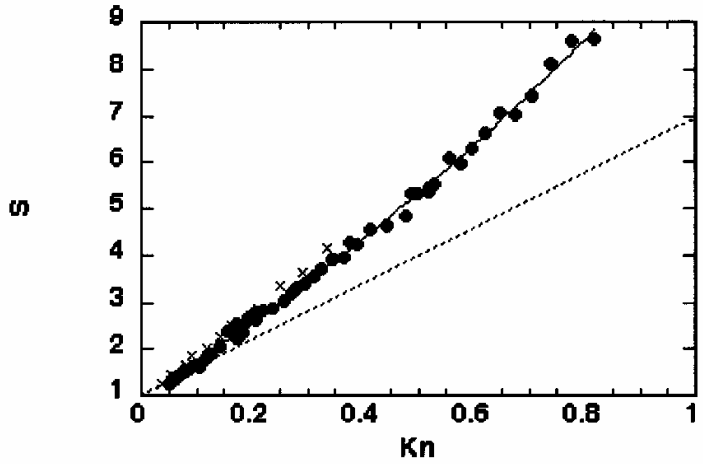

FIG. 5. Evolution of the slip coefficient S, for helium; the crosses represent Colin *et al.* data; the dashed line represents the full accommodation limit ($\sigma=1$), without second-order effects. The full line is the fit by a polynom of degree 2.

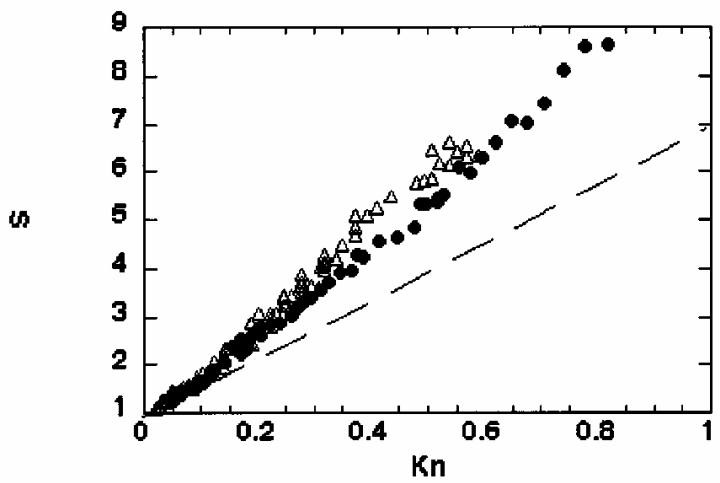

FIG. 7. Evolution of the slip coefficient S, for helium (disks) and nitrogen (triangles), displayed on the same plot, so as to compare measurements.

The plot represents a dimensionless number S, defined by :

$$S = \frac{12 Q \mu P_O L}{P_m \Delta P}$$

where Q is the volumetric flow-rate, μ the fluid viscosity, L the channel length, Pm the mean pressure along the channel, and ΔP the pressure drop. The Maxwell theory, with σ=1, is shown on the Figures. From such measurements, we estimate the accomodation factor for Helium to be equal to 0.91±0.03 and for Nitrogen 0.87. The deviation from the first order b.c. is obvious. For both gases it was found that the averaged limiting Kundsen number

$$Kn_s \approx 0.3 \pm 0.1$$

Beyond this number the second order effect becomes significant

A general boundary condition for liquid flow at solid surfaces

Peter A. Thompson* & Sandra M. Troian†

* *The Celerity Group, 20 Nassau Street, Suite 209, Princeton, New Jersey 08542, USA*

† *Department of Chemical Engineering, Princeton University, Princeton, New Jersey 08544, USA*

Molecular dynamics simulations

The degree of slip at the boundary conditions depends on a number of interfacial parameters including the strength of the liquid-solid coupling, the thermal roughness of the interface, and the commensurability of wall and liquid densities.

The amount of momentum transfer at the wall/fluid interface decreases as the relative surface energy corrugation of the wall decreases -slip develops

Efficient momentum transfer corresponds to no-slip condition.

ε^{wf} Energy and

σ^{wf} Length scales

$$\Delta V = L_s \dot{\gamma}$$

Navier boundary condition

ΔV Velocity difference between solid and liquid

L_s Slip length

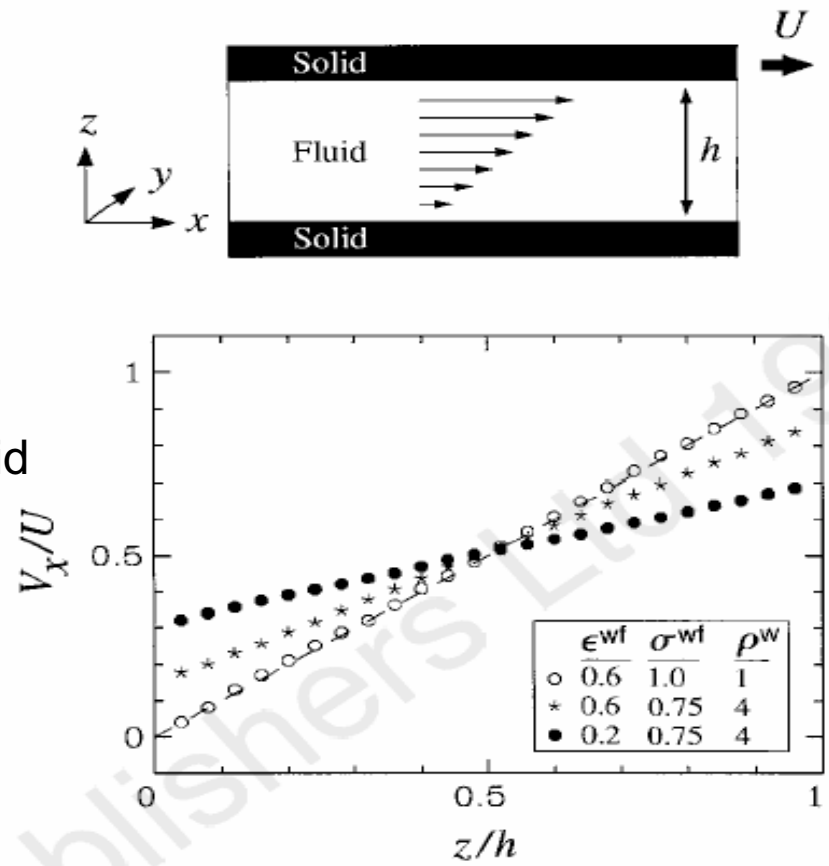

Figure 1 Steady-state flow profiles and schematic of the Couette flow geometry. The Couette cell measured $12.51\sigma \times 7.22\sigma \times h$ where h varied from 16.71σ to 24.57σ The number of fluid molecules ranged from 1,152 to 1,728, respectively. The $\hat{\mathbf{x}}$-direction of the cell is aligned along the $[11\bar{2}]$ orientation of the face-centred cubic lattice comprising the wall, and periodic boundary conditions are imposed along $\hat{\mathbf{x}}$ and $\hat{\mathbf{y}}$. The flow profiles were obtained for systems with $U = 1.0\sigma\tau^{-1}$, $h = 24.57\sigma$, and walls characterized by the indicated density and Lennard–Jones parameters. Values for ϵ^{wf}, σ^{wf} and ρ^{w} (see text) are in units of ϵ, σ and ρ, respectively. Following an equilibration period of $\sim 100\tau$, the profiles were computed by averaging the instantaneous particle velocities within bins of width $\sim 1\sigma$ spanning the distance between the two walls. The duration of the averaging varied from 250τ to $7{,}000\tau$ depending on the signal-to-noise ratio. Accurate resolution of flows with $\dot{\gamma} < 0.01\tau^{-1}$ typically required $> 2{,}500\tau$ of averaging. The dashed line indicates Couette flow with a no-slip boundary condition.

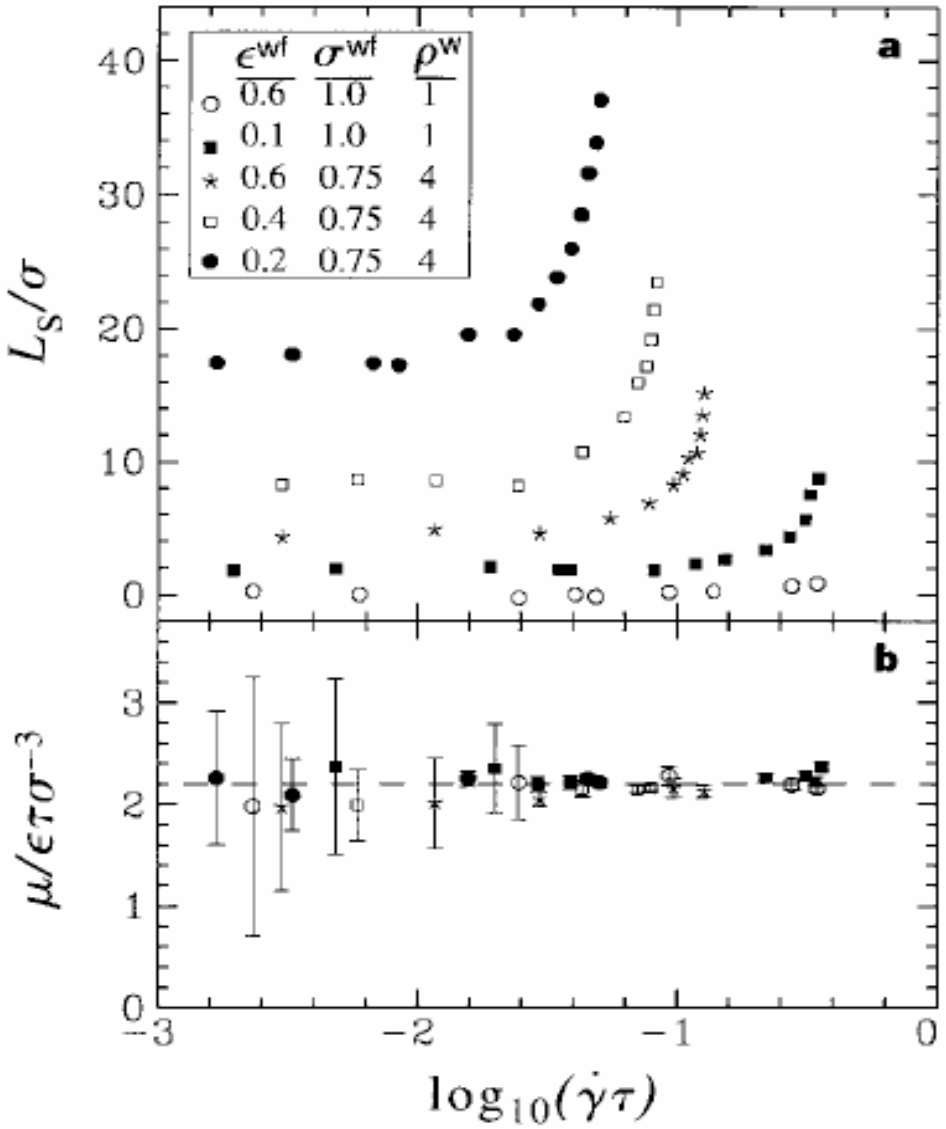

Figure 2 Variation of the slip length L_s (panel **a**) and viscosity μ (panel **b**) as a function of shear rate for systems with the indicated interfacial properties. L_s was computed from the definition $L_s = \Delta V_x/\dot{\gamma}$, which for Couette flow reduces to $(U/\dot{\gamma} - h)/2$. μ was computed from the relation $\mu = P_{zx}/\dot{\gamma}$, where P_{zx} is the zx-component of the microscopic stress tensor averaged across the cell[19].

$$\tau = \left(m\sigma^2/\varepsilon\right)^{1/2}$$

Characteristic time of the Lennard-Jones potential (microscopic)

$$\mu = const$$

$$\dot{\gamma} \geq 2\tau^{-1}$$

-non-Newtonian response can be expected

$\dot{\gamma}_c$ -critical shear rate at which Slip length diverges

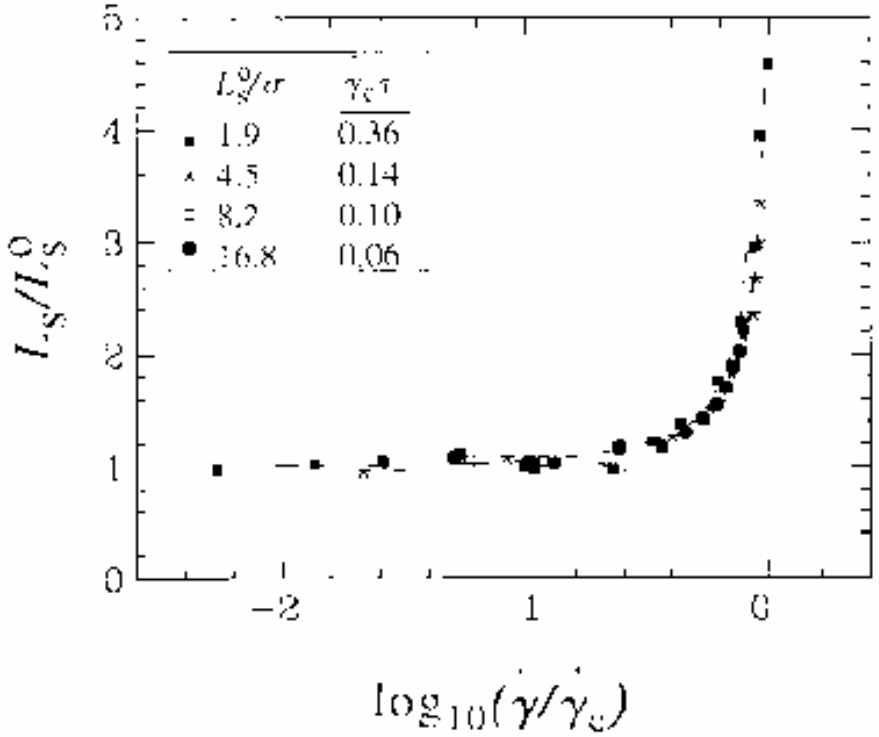

Figure 3 Master curve describing the flow boundary condition. The data is the same as that shown in Fig. 2a with L_s and $\dot{\gamma}$ scaled by the indicated values of L_s^0 and $\dot{\gamma}_c$. The dashed line represents $L_s = L_s^0(1-\dot{\gamma}/\dot{\gamma}_c)^{-1/2}$.

$$L_s = L_s^0(1-\dot{\gamma}/\dot{\gamma}_c)^{-\alpha}$$

$$\alpha = 1/2$$

Particle in driven periodic potential also shows ν_c

$$\dot{\gamma}_c \propto R^{3/4}$$ where ***R*** is roughness characteristic

Shear-dependent boundary slip in aqueous Newtonian liquid

V.Craig et al, PRL **87**, 054504 (2001)

$$\theta_{adv} = 70^{\circ}; \theta_{rec} = 40^{\circ}$$

AFM is used

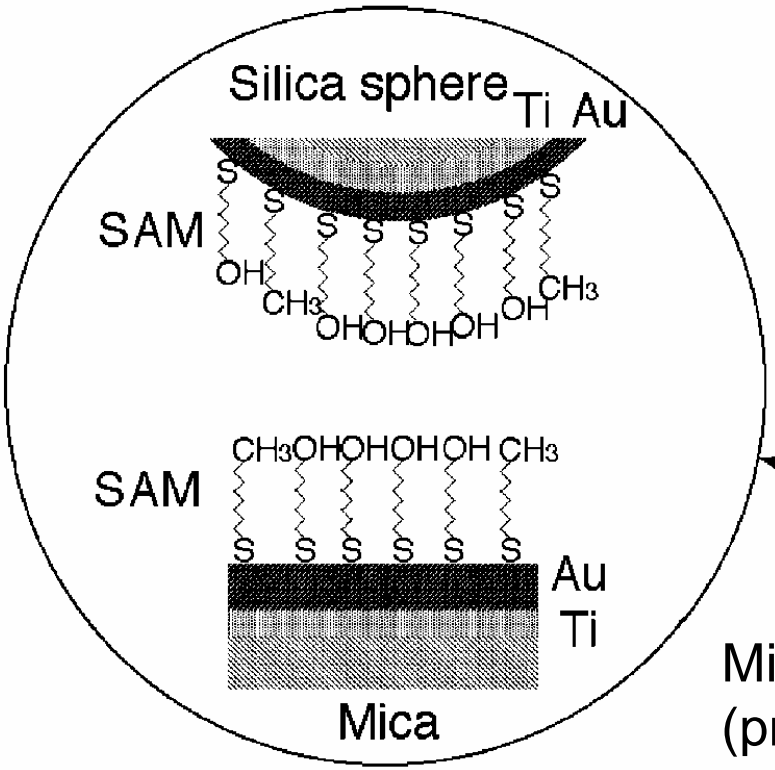

10.4 micron silica sphere gold coated and thiol monolayer (SAM)

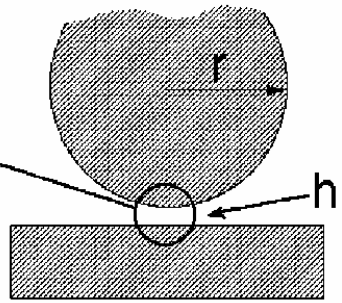

Mica gold coated and thiol monolayer (provides control of roughness and wettability

FIG. 1. Schematic representation of the employed sphere-plane system. The sphere of radius r is separated from the flat surface by h at the point of closest approach.

$$F_h = 6\pi\eta r V \lambda$$

$$\lambda = \frac{r}{r+h}$$

no-slip **(1)**

(force on sphere approaching flat surface)

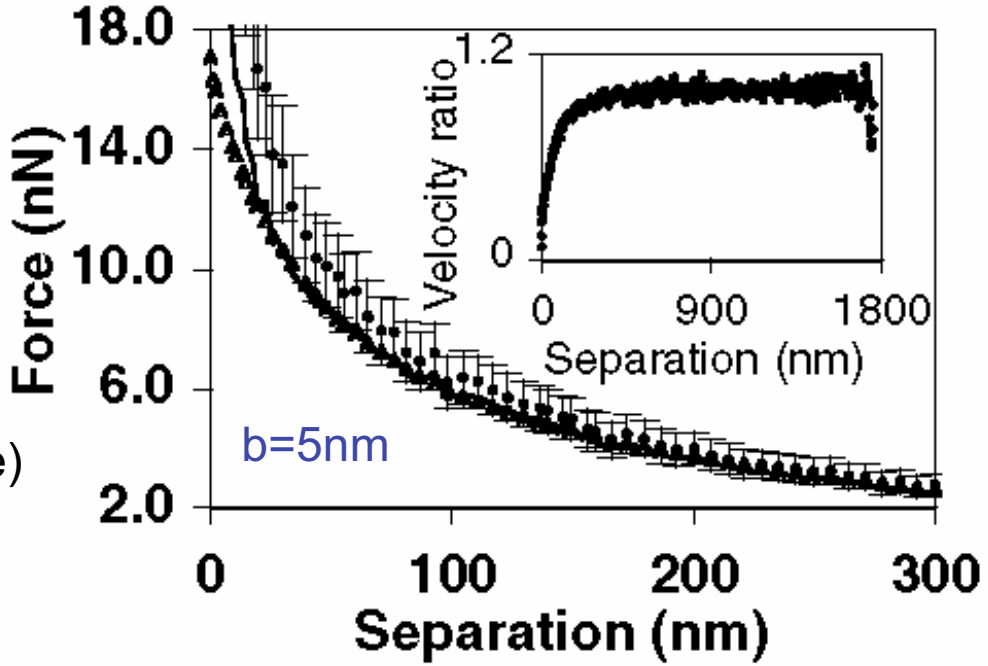

FIG. 3. Measurement of the hydrodynamic drainage force in a sucrose solution. The experimental data (empty triangles) are presented together with the no-slip theory (circles, with error bars) and the slip theory (line). The piezodrive rate is 21 600 nm/s and the viscosity of the sucrose solution is 19.2 mPa s. The fitted slip length is 5 nm. In the inset we report the ratio of the approach and drive velocity.

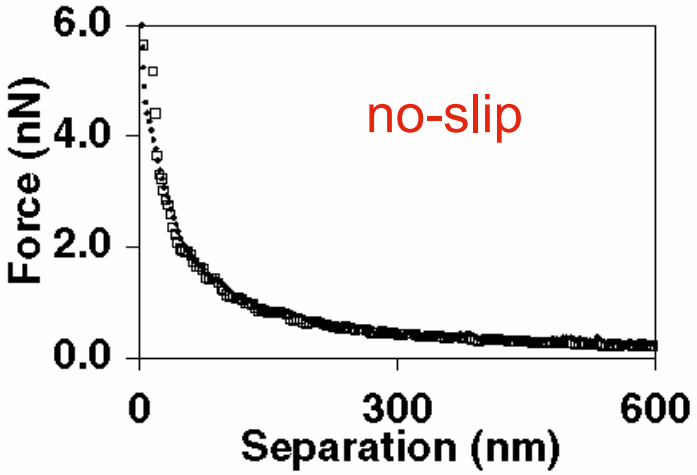

FIG. 2. Measurements of the hydrodynamic drainage force in a sucrose solution. The piezodrive rate is 2400 nm/s and the viscosity of the sucrose solution is 27.0 mPa s. The experimental data (circles) are presented together with the Brenner theory prediction (empty squares).

$$F_h = \frac{6\pi r^2 \eta V}{h} f^* \quad \text{slip, } b\text{-slip length} \quad \textbf{(2)}$$

$$f^* = \frac{h}{3b}\left[\left(1+\frac{h}{6b}\right)\ln\left(1+\frac{6b}{h}\right)-1\right]; (h<r)$$

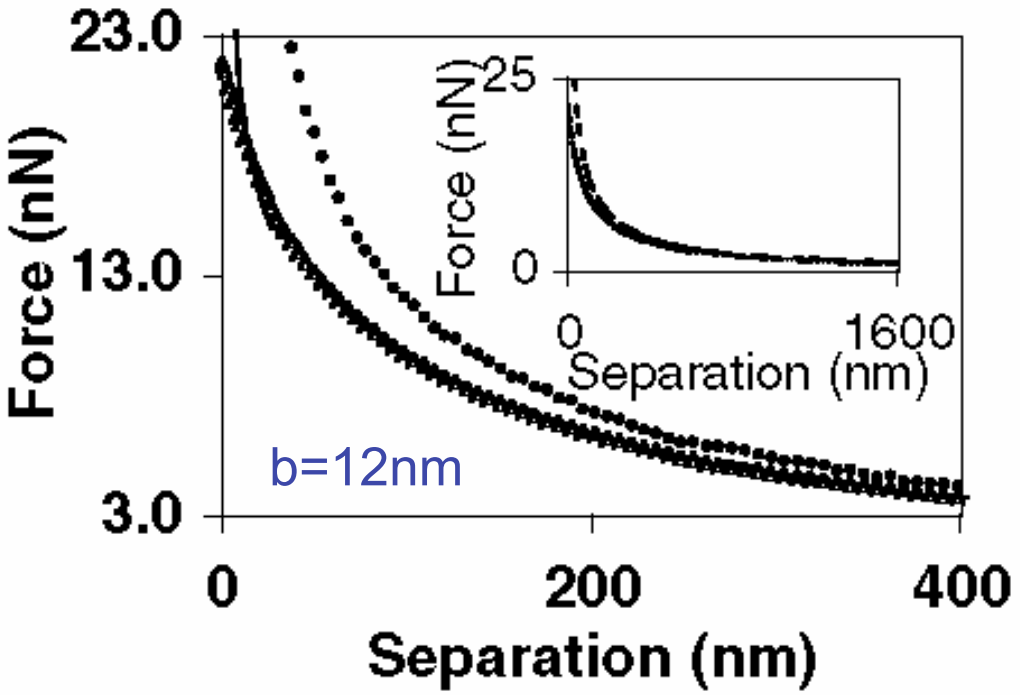

FIG. 4. Measurement of the hydrodynamic drainage force in a sucrose solution. The experimental data (empty triangles) are presented together with the no-slip theory (circles, with error bars) and the slip theory (line). The piezodrive velocity is 21 600 nm/s and the viscosity of the sucrose solution is 38.9 mPa s. The fitted slip length is 12 nm. In the inset the full scale experimental data (solid line) and the full scale Brenner theory (broken line) are presented.

High rate approach is crucial to observe slip boundary conditions!

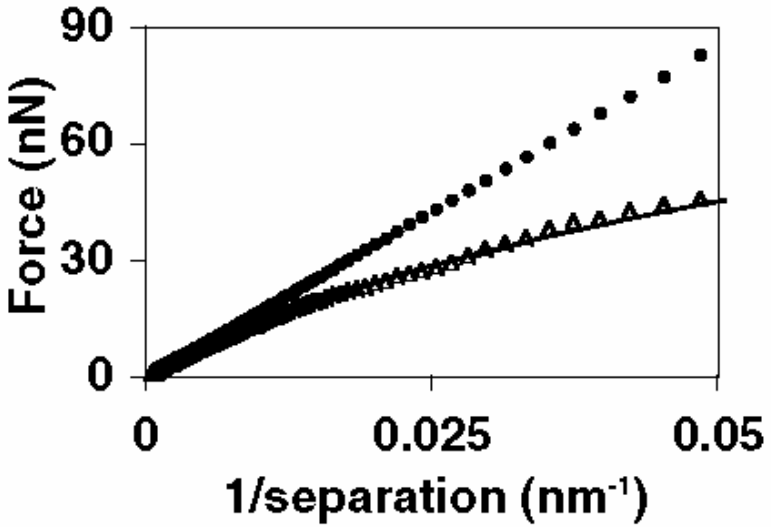

FIG. 5. Hydrodynamic force versus inverse of separation. The same data as in Fig. 4 are reported. The experimental force data are divided by the velocity ratio (see Fig. 3) to allow comparison with theories.

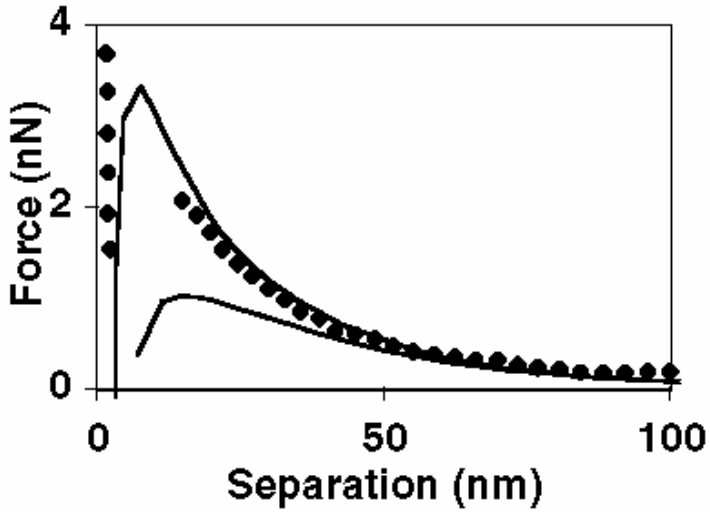

FIG. 7. Measurement of the typical equilibrium forces present in the system. The surface forces (diamonds), measured at low approach velocity in a 46% sucrose solution w/w, viscosity 10.2 mPa s, are fitted using the DLVO theory, for both the constant charge (upper curve) and constant potential (lower curve) boundary conditions.

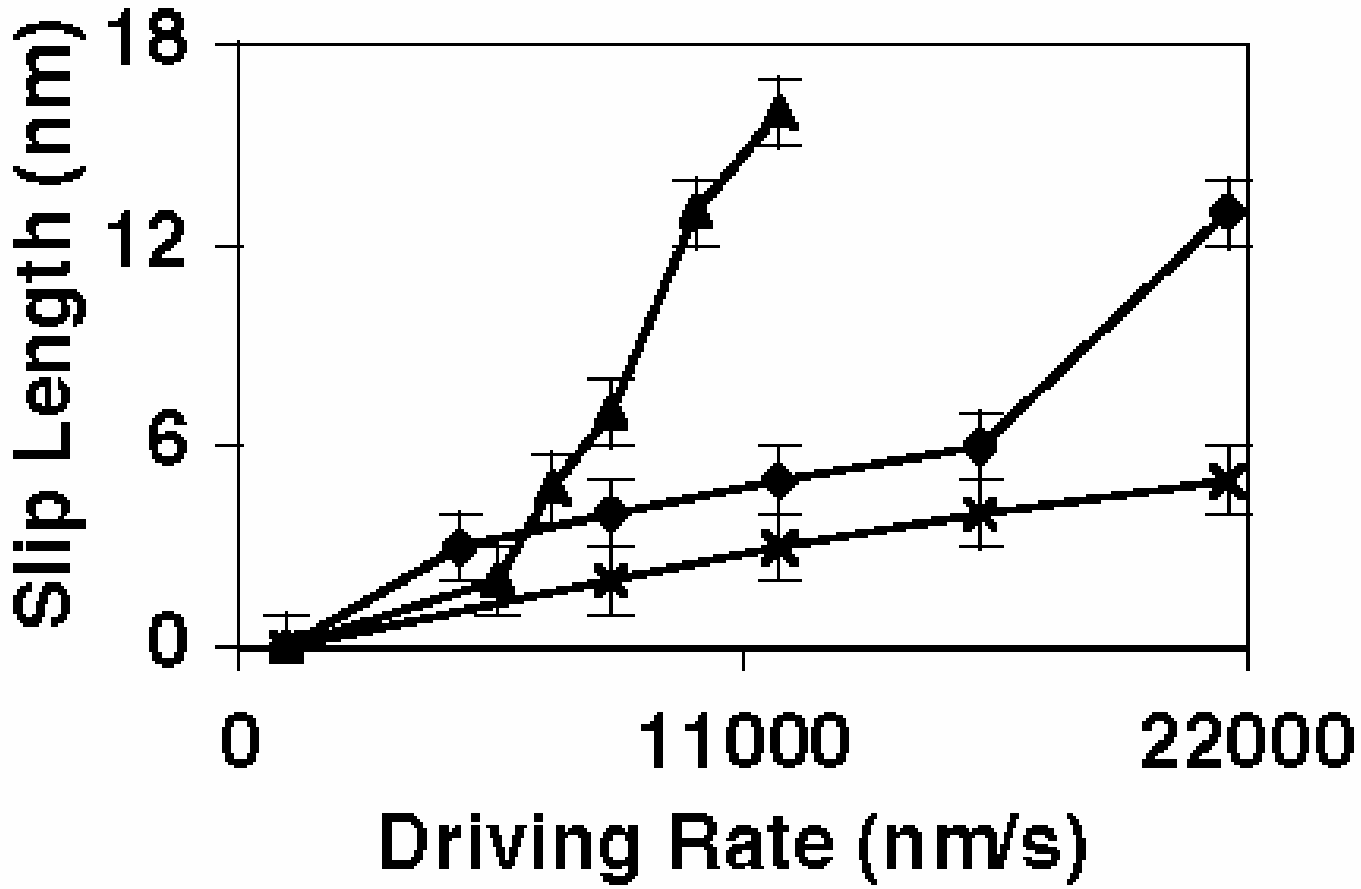

FIG. 6. Slip length versus driving rate. The sucrose solutions have viscosities of 19.2 mPa s (crosses), 38.9 mPa s (diamonds), and 80.3 mPa s (triangles). The lines are included to guide the eye.

Rate-dependent slip of Newtonian liquid at smooth surfaces

Y.Zhu&S.Granick,PRL **87**, 096105 (2001)

There is a critical value of the flow rate above which partial slip appears

It is the first direct measurements in which velocity of the moving object is varied over a wide range and the conclusions are:

- amount of slip is strongly dependent on velocity
- the onset of slip varied systematically with contact angle

$R \approx 2cm$ mean radius of curvature

$\boldsymbol{D}$ -spacing

F_H -hydrodynamic force

The **no-slip boundary conditions combined with the Navier-Stokes** equations give to the first order the following expression for the hydrodynamic force due to squeezing of a fluid out of the gap. This expression is known as **the Reynolds equation**

$$F_H = f^* 6\pi R^2 \eta (1/D)(dD/dt)$$

$f^* \neq 1$ -the non-dimensional parameter that quantifies deviation from the classical prediction (that was confirmed on wetted surface)

The analogous prediction is for oscillated surface spacing. Then oscillatory drive generates an oscillatory force whose Peak is denoted as $F_{H,peak}$. The peak velocity is $v_{peak} = d\omega$

Modified surface force apparatus with lock-in, tetradecane against absorbed surfactant and SAM, and water against SAM have been used.

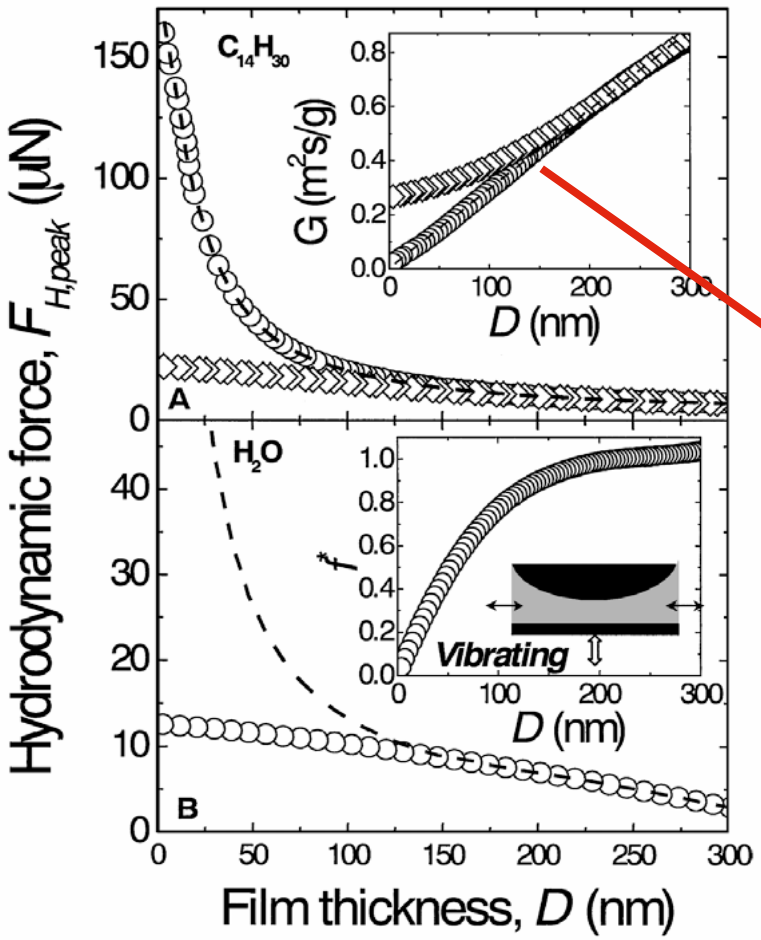

FIG. 1. Hydrodynamic force between crossed cylinders. $F_{H,\mathrm{peak}}$, is plotted against surface separation D for tetradecane (upper panel) and deionized water (bottom panel) undergoing 1 nm spacing vibrations at 63 rad s^{-1}. In the top panel, the surface was wetting (mica; circles) or partially wetting with contact angle ≈44° (OTE; diamonds). A schematic diagram of the experiments is shown in the bottom panel. The data are compared to the hydrodynamic force expected from the no-slip boundary condition, Eq. (1) (dashed lines). The inset of each panel shows the damping function, $G = (6\pi R^2 \nu_{\mathrm{peak}})/F_{H,\mathrm{peak}} = D/\eta$, plotted against D. The reciprocal of the slope in the linear portion of the inset gives the known viscosity of these fluids. Given the no-slip boundary condition and a Newtonian fluid, G should extrapolate to the origin.

Tetradecane, oil with low viscosity:

- between mica-wetting (circles)
- OTE -partial wetting (diamonds)
- dashed line-classical theory

$$G=(6\pi R^2 v_{peak})/F_{H,peak}=D/\eta$$

For partial wetting force was less than for wetting case. Water gives similar results

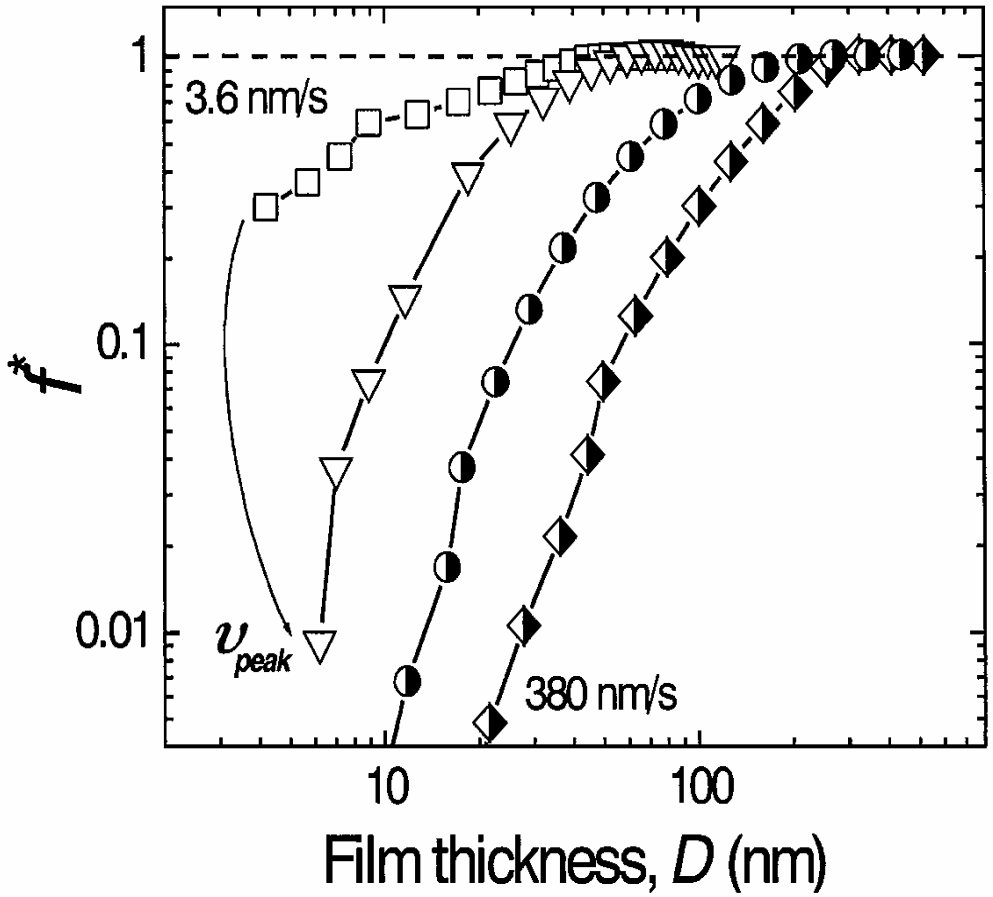

FIG. 2. On log-log scales, f^* is plotted against D for deionized water between partially wetting (OTE-coated) at peak velocity 3.6 nm s^{-1} (squares, 1 Hz), 40 nm s^{-1} (triangles, 1 Hz), 100 nm s^{-1} (circles, 10 Hz), and 380 nm s^{-1} (diamonds, 10 Hz). Given the no-slip boundary condition, $f^* = 1$. To observe $f^* < 1$ shows that flow was easier than expected from that assumption.

4 values of peak velocity

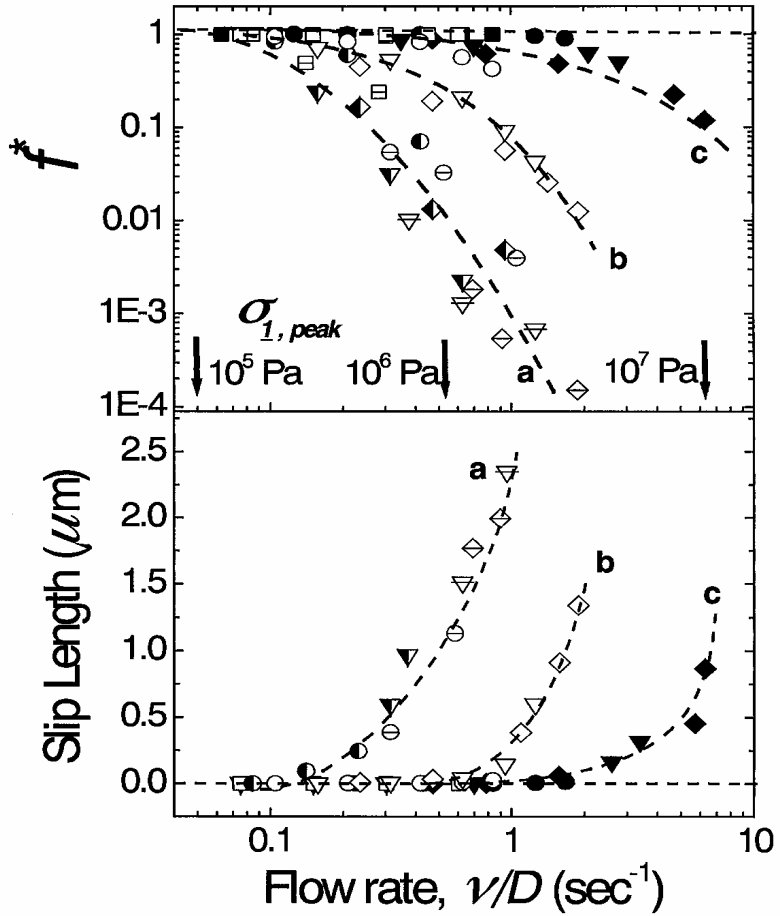

FIG. 3. On log-log scales, f^* (top panel) is plotted against v_{peak}/D for (a) deionized water between OTE (cross or semi-filled symbols), contact angle $\approx 110°$, (b) tetradecane between OTE (open symbols), contact angle $\approx 44°$, and (c) tetradecane containing 0.2% hexadecylamine between mica (filled symbols), contact angle $\approx 12°$. At the thickness 50 nm (squares), 24 nm (circles), 18 nm (triangles), and 8 nm (diamonds), the frequency was 6.3 rad s^{-1} or 63 rad s^{-1} (cross-filled symbols). The peak hydrodynamic stresses of 10^5, 10^6, and 10^7 Pa are indicated at the corresponding flow rate points on the abscissa. The bottom panel compares the slip length, which is equivalent to f^* as described in text. Shear rate is, if the stick boundary condition holds, proportional to flow rate in a crossed cylinder geometry by a geometrical factor of magnitude between 10^3 and 10^4 that depends on D [26], $\gamma_{max} = A\sqrt{R/D}\, v_{peak}/D$, where $A = (27/128)^{1/2}$.

$$f^* = 2 \times \frac{D}{6b}\left[(1+\frac{D}{6b})\ln(1+\frac{6b}{D}) - 1\right]$$

b is the slip length

Peak velocity changed by more than two orders of magnitude and the data for different velocities are collapsed being compared for the same flow rate.

Limits of the hydrodynamic no-slip boundary condition

Slippery question

Y. Zhu & S. Granick, PRL **88**, 106102 (2000)

First studies in which roughness was varied systematically at the nanometer level

Technique is the same as in previous studies

Copolymer of polystyrene (M=55400) and polyvinylpyridine (PS/PVP);
Layers: (i) OTS, (ii) PS/PVP-OTE 80% Coverage, (iii) PS/PVP-OTE 20%

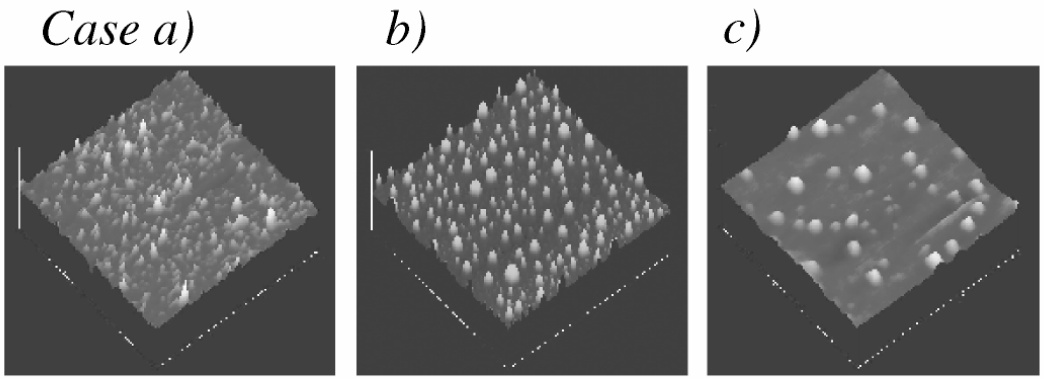

FIG. 1. The scheme of flow over a rough surface is shown schematically in the top portion of this figure. In the bottom panels, AFM images are shown of the following cases: (a) self-assembled OTS layers; (b) PS/PVP-OTE layers (surface coverage ~80%); (c) PS/PVP-OTE layers (surface coverage ~20%). Each AFM image concerns an area 3 μm × 3 μm.

Roughness: (see also next fig.)

OTS-6nm-squares
PS/PVP-OTE-80-3.5nm-cirles
PS/PVP-OTE-20-2nm-down triangles
Smooth OTE-0.2nm-diamonds
Thiol on Ag-0.5nm-up triangles
Thiol on Ag-1.2nm-hexagons

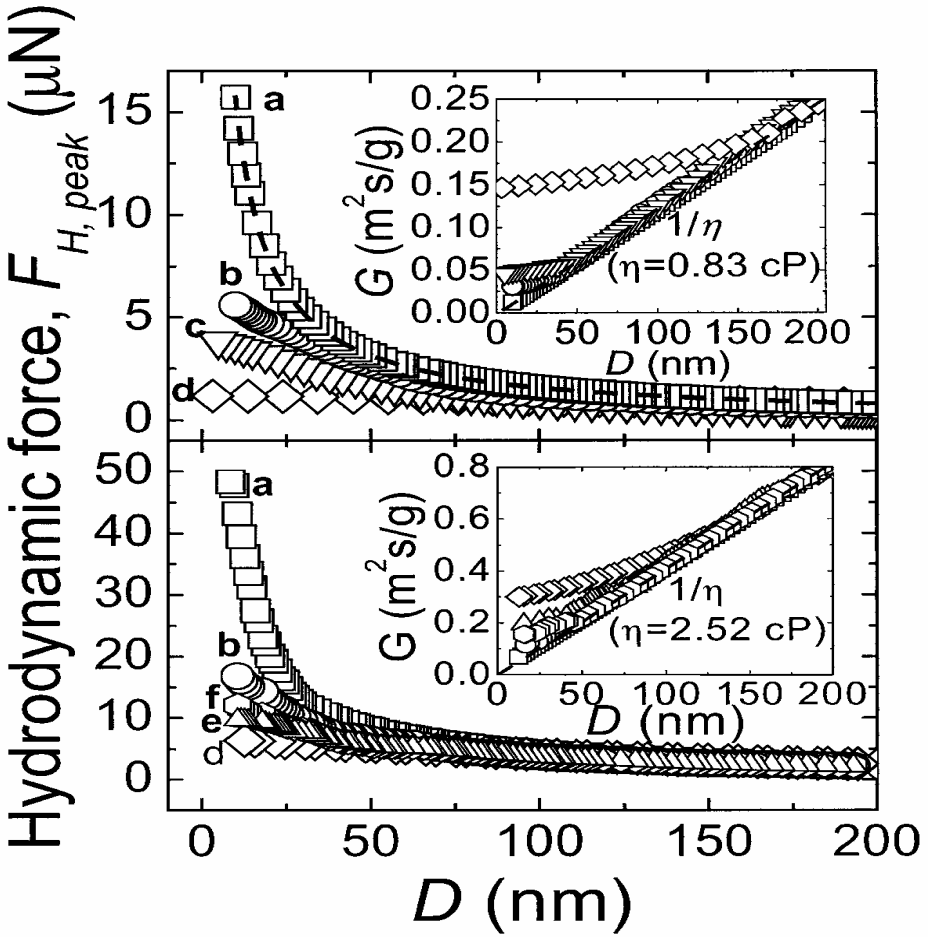

FIG. 2. Hydrodynamic force between crossed cylinders, $F_{H,\mathrm{peak}}$, is plotted against surface separation D for tetradecane (bottom panel) and deionized water (top panel) undergoing 1 nm vibrations at 63 rad s^{-1} ($v_{\mathrm{peak}} = 63$ nm s^{-1}). The rms roughness was 6 nm (case a; squares), 3.5 nm (case b; circles), 2 nm (case c; down triangles), 1.2 nm (case f; hexagons), 0.6 nm (case e, up triangles), and molecularly smooth (case d; diamonds). The inset in each panel shows the damping function, $G = 6\pi R^2 v_{\mathrm{peak}}/F_{H,\mathrm{peak}} = D/\eta$, plotted against D. The reciprocal of the slope in the linear portion of the inset gives the known viscosity of these fluids. Given the no-slip boundary condition and a Newtonian fluid, G should extrapolate to the origin. The observed curvature implies a breakdown of the no-slip boundary condition.

water

dashed line-theory

tetradecane

The rougher the solid, the better

Agreement with no-slip b.c.

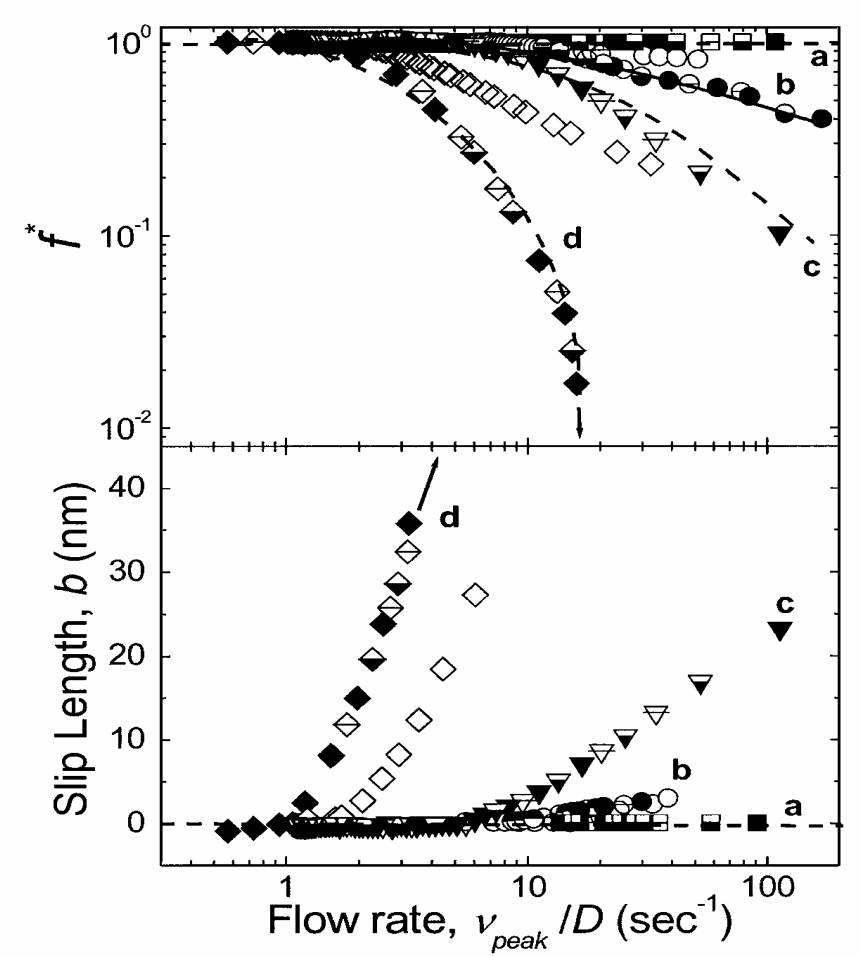

FIG. 3. As a function of logarithmic flow rate, v_{peak}/D, f^* [top panel; f^* is defined in Eq. (1)] and the equivalent slip length (bottom panel) are plotted, for deionized water (filled symbols) and tetradecane (open symbols) flowing between surfaces whose different levels of rms roughness are identified in Table I. Symbols are the same as in Fig. 2. The data, taken at different amplitudes in the range of 0.3–1.5 nm and frequencies in the range 6.3–250 rad sec^{-1}, are mostly not distinguished in order to avoid clutter, since their successful collapse as a function of v_{peak}/D was shown in detail for smooth surfaces previously [12]. To illustrate the similarly successful collapse for these rough surfaces, data taken at the two frequencies 6.3 rad sec^{-1} (cross filled symbols) and 31 rad sec^{-1} (semifilled symbols) for water are included explicitly. In the bottom panel, the slip length (b) was calculated as described in the text.

As in previous studies for smooth surfaces the data are collapsed for different roughness
Also deviation from no-slip condition larger for smaller roughness

Dependence on shear rate is suggested by de Gennes to be explained as shear induced vapor bubble nucleation

Critical shear rate for onset slip

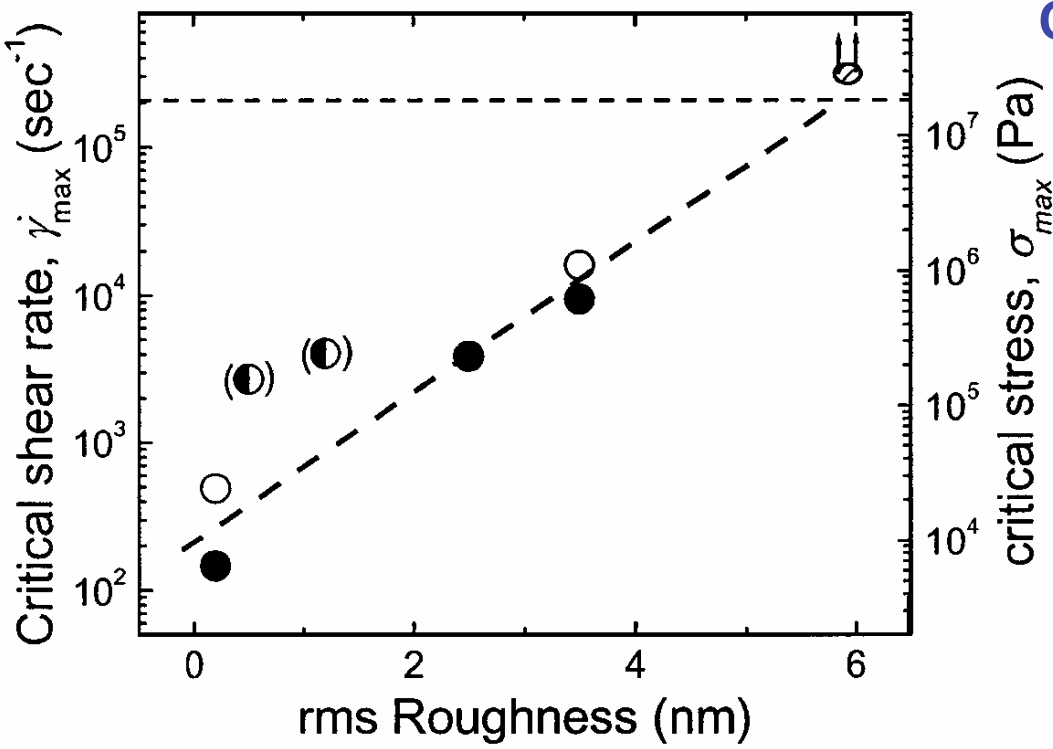

$$\dot{\gamma}_{\max} = A(R/D)^{1/2} v_{peak}/D; A = (27/128)^{1/2}$$

$$\sigma_{peak} = 3\eta R v_{peak}/D^2$$

FIG. 4. The critical shear rate for onset of slip (left ordinate) and critical shear stress (right ordinate) are plotted semilogarithmically against rms roughness for flow of deionized water (solid symbols) and tetradecane (open symbols for cases *a*–*c* in Table I and semifilled symbols for cases *e* and *f*). The data in parentheses indicate the asymmetric situation of cases *e* and *f* on one side and case *a* on the other side—one surface was rough and the opposed surface was atomically smooth. Shear rate and shear stress at the coincident apex of the cross cylinders were calculated using known relations based on continuum hydrodynamics [21].

Conclusions

The slip length larger at

- hydrophobic surfaces (non-wetting or partial wetting)
- smooth surface
- shear rate above the critical

In the non wetting case, consistency between slip length measurements is not established yet

Slip lengths

D.C. Tretheway *et al.* **1000 nm ± 450 nm** water / OTS on glass (PIV, 2001)
Y. Zhu *et al* **2000 nm** *dependent* water / OTE on mica (SFA, 2001)
C.H. Choi *et al.* **100 nm ± 50 nm** water / OTS on glass (P vs. Q, 2003)
C. Cottin-Bizonne *et al.* **20 nm ± 3 nm** water / OTS on glass (SFA, 2003)
T. Schmatko *et al.* **450 nm ± 200 nm** hexadecane / sapphire (NFLV, 2003)
& O. Vinogradova *et al* **10 nm ± 1 nm** water / Polystyrene (AFM, 2003)
P.Joseph, P. Tabeling **50 ± 50 nm** water / OTS on glass (PIV, 2005)*
* P.Joseph, P.Tabeling, Phys. Rev. E, April 2005

Next generation of the experiment

Measurements of *b* (the slip length) have been performed in various situations, for a variety of solid surfaces, and several fluids. Results indicate the slip length is on the order of **micrometers, or fractions of micrometers**, the main parameters being the **strength of the interactions liquid-solid** and the **roughness of the substrate**.

These values are much larger than typical intermolecular scales. There is no clear understanding, at the moment, for this set of observations. A possibility suggested by de Gennes is that a gaseous layer nucleates at the interface between the fluid and the solid, favoring slippage. This proposal remains to be investigated experimentally.

Our objective is to make progress on the measurement of slip lengths, by developing a direct method of determination of the velocity (using PIV), in thin micro-channels.

The technique we present here allows, with ±100 nm accuracy , to measure the slip length of water flowing over glass; the same technique is applied for silicon substrates functionalized with OTS.

Direct measurement of the apparent slip length

Pierre Joseph* and Patrick Tabeling
Laboratoire MMN, UMR CNRS-ESPCI 7083, 10 rue Vauquelin, F-75231 Paris Cedex 05, France
(Received 22 November 2004; published 31 March 2005)

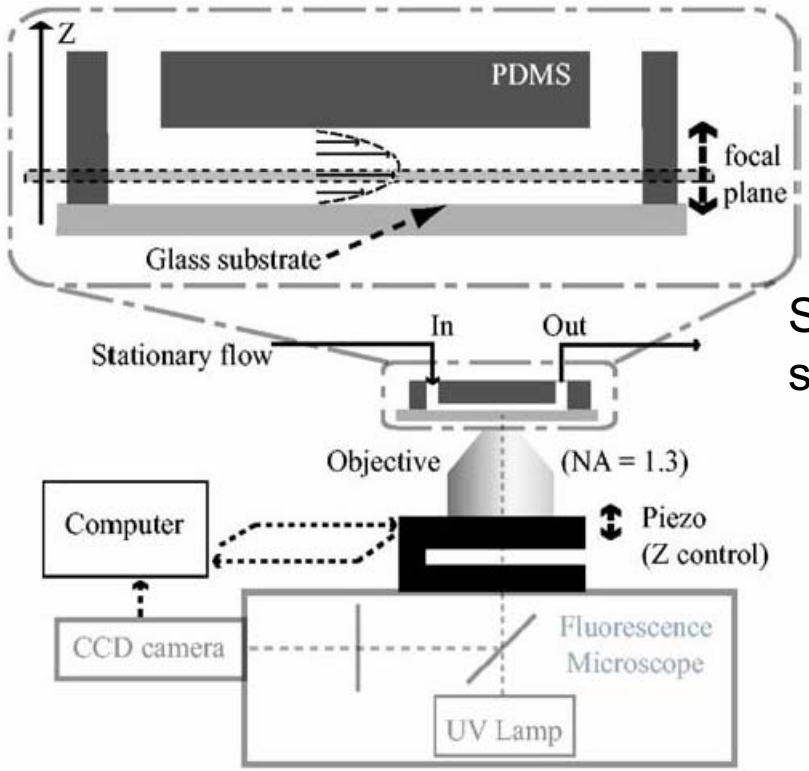

FIG. 1. Scheme of the experiment. A stationary flow of fluorescent tracers in deionized water is imposed in a PDMS/glass microchannel. The lower surface, a microscope coverslip, can be chemically modified before enclosure. The focal plane is controlled with a piezo, a large numerical aperture objective allowing a narrow depth of field. Velocity is measured by particle image velocimetry. The entire velocity profile is determined thanks to a scan on z position.

Smooth hydrofobic surface the slip length reaches several microns (!)-Granick et al

PIV with unprecedented precision to define the slip length and it is below 100nm

$$10\,\mu m \times 100\,\mu m \times 1cm$$

Hydrophilic bare glass and hydrophobic grafted glass (OTS or CDOS) were used

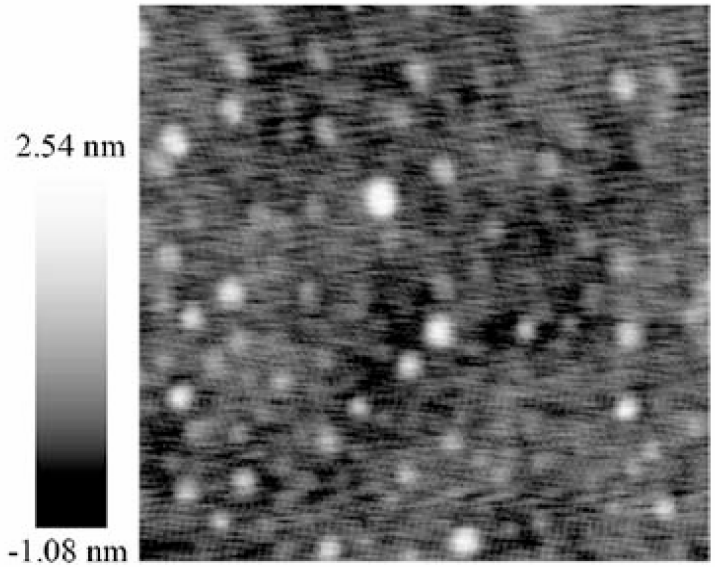

FIG. 2. 500 nm × 500 nm tapping mode AFM image of a hydrophobic surface (OTS grafted on glass). rms roughness is 0.45 nm. This surface is the one used in measurements of Fig. 4(b).

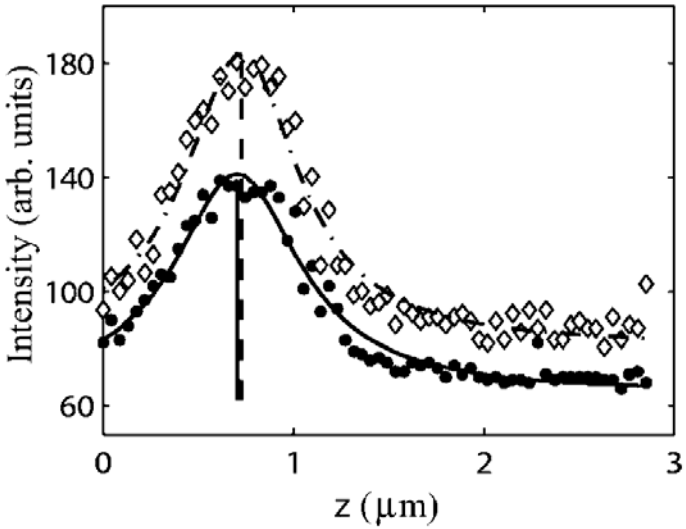

FIG. 3. Determination of the wall position: Averaged intensity of each adsorbed particle is fitted with a Lorentzian. The particle radius is removed to the mean z position of the peaks to give the actual glass location within ±30 nm.

$$\Delta p \leq 5 mbar$$

Imaged plane

$$500 nm \times 12 \mu m \times 25 \mu m$$

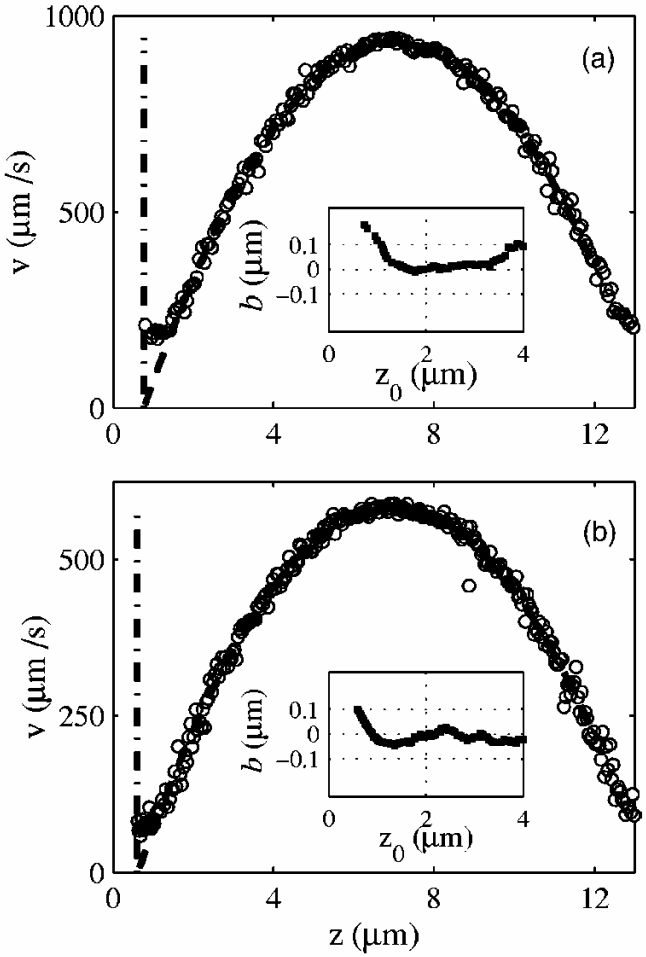

Hydrophilic glass surface

Hydrophobic OTS on glass surface

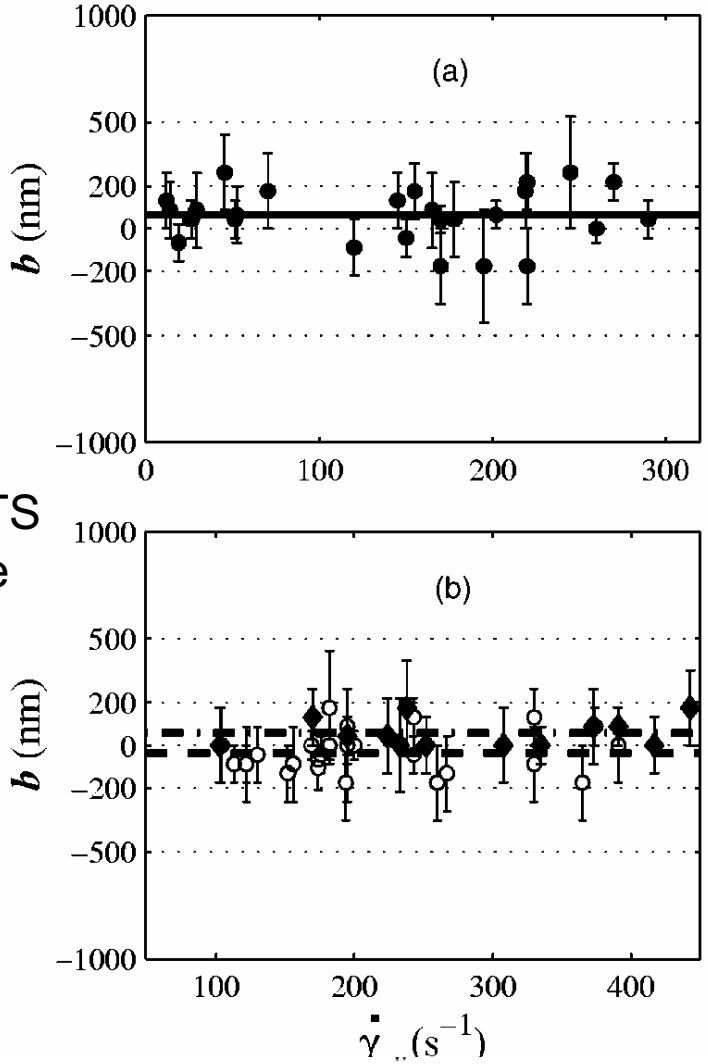

FIG. 4. (a) Velocity profile and parabolic fit for a smooth and hydrophilic substrate (glass). The dashed-dotted line shows the position of the solid wall. The inset corresponds to the variation of the slip length when changing the origin z_0 of the fit zone, for a fixed end z_f=12 μm. (b) Averaged velocity and parabolic fit for a hydrophobic monolayer of silane (OTS) grafted on glass.

FIG. 5. Slip length b as a function of the shear rate at the wall, for water flowing on different surfaces: (a) hydrophilic glass and (b) hydrophobic monolayers of OTS on glass (white circles) and CDOS on glass (black diamonds).

Slip length is difference between measured wall position and extrapolation of parabola